Magnetically Suspended Reaction Sphere with One-axis Hysteresis Drive

Lei Zhou, Mohammad Imani Nejad, David L. Trumper

Dept. of Mechanical Engineering, Massachusetts Institute of Technology
77 Massachusetts Avenue, Cambridge, MA, USA

{leizhou, m_imani, trumper} @mit.edu

***Abstract*—We have designed, built and tested a magnetically suspended reaction sphere with one-axis hysteresis drive (1D-MSRS) in the Precision Motion Control Lab at MIT. This project is aiming at two goals: (a) exploring the possible design of a magnetically suspended reaction sphere for small spacecraft's attitude control; and (b) evaluating the performance of a hysteresis motor for the reaction wheel/sphere application. The 1D-MSRS is a motor with spherical rotor, which is magnetically suspended in all translational directions, and is driven by hysteresis motor about vertical axis. For the suspension of the sphere, single dimensional magnetic levitation in vertical direction and bearingless motor around the rotor are combined. An equivalent circuit model of the hysteresis motor is used to analyze the motor's dynamic behavior. Good agreements between computed and measured motor performance validates the model, which provides a useful simulation tool for further MSRS modeling and control. Test results of the 1D-MSRS show that a starting torque of 8.15 mNm is achieved at 0.7 A zero-peak excitation current, and with this excitation the sphere can run up to 12,000 rpm synchronously in lab with the existence of air drag.**

I. Introduction

In a spacecraft's flight control, the Attitude and Orbit Control System (AOCS) of the spacecraft is responsible for the high precision of control in orbit. When the spacecraft is maneuvering, it requires an external force, or torque, which is often provided by a minimum of three reaction wheels (often 4-5 wheels are used for optimization and redundancy [1]). By accelerating the appropriate wheels, the system can produce a zero-mean torque about any axis to the spacecraft, and momentum can be stored as well [2]. Such wheels are often used for both spacecraft attitude control [3] and large angle slewing maneuvers [4]. Other applications include vibration compensation and orientation control of solar arrays [5], as well as energy storage.

As an alternative to a combination of several reaction wheels, we propose to use of a magnetically levitated reaction sphere (MSRS) for satellite's attitude control. Our alternate version is that the sphere can be angularly accelerated about any axis by a three dimensional (3D) motor, making the attitude of the spacecraft in all axes controllable by a single device. Due to its symmetry, a sphere can always gives the same inertia, independent of its rotational axis. Thus using reaction sphere can reach smaller size and mass, which is an essential consideration for space device design. Also, magnetic suspension eliminates imbalance, so the vibrations emitted by the reaction wheel that degrade the performance of precision instruments in space are suppressed. Mechanical friction is also eliminated by the magnetic bearing, and thus low steady-state power consumption may be possible. This also enables it work without lubrication and can be expected to have longer maintain-free lifespan. Furthermore, the rotation of a sphere has no gyroscopic coupling between the rotations about the three axes, which potentially enables better control possibilities.

The idea of a reaction sphere was proposed more than two decades ago [6], but to our knowledge none have reached a ready-for-commercialization technology. To our understanding, this is mainly due to the difficulties of 3D angular position sensing for spherical rotor and the complexity due to coupling of fields by stator segments and between bearing and motor functions. In recent years several spherical motors, mainly for robotics application, have been developed [7] [8] [9] [10] [11] [12]. These design often include a mechanical shaft coupling that induces a rotational singularity, which prevents them from directly being used as an all degree-of-freedom actuator for attitude control. A permanent-magnet-motor-based reaction sphere is presented in [13]. This design successfully solved the problem of sensing and field coupling, which makes it a good actuator about all axis. But the complexity of its magnetic structure may prevent it from being suitable for small satellites application, and the strength of the rotor limits its maximum rotational speed, which may limit the performance of the actuator.

Among many motor driving principles, the hysteresis motor is receiving increasing attention due to its advantages of simple structure, vibration-free operation, self-starting and constant torque production in starting. Another distinct feature of this motor is that its rotor can be made out of a single piece of hard and strong steel, which allows the rotor to stand large stresses and makes this motor concept attractive for high-speed applications. Reference [14] reported the performance of several hysteresis motors of different scales, and the results make us believe that this kind of motor concept may demonstrate good performance in reaction wheels. However, to the best of our knowledge, the hysteresis motor has not been introduced to the development of reaction wheels until now.

Aiming at the dual goal of exploring the design for a magnetically suspended reaction sphere and evaluating hysteresis motor performance for reaction wheels application, we decide to focus this project on the development of a magnetically suspended reaction sphere with one-axis hysteresis drive (1D-MSRS). The hardware demonstrates a motor with a spherical rotor driven by hysteresis motor, and is magnetically suspended in all translation directions. For the suspension of the sphere, single dimensional magnetic levitation in vertical direction and bearingless motor around the rotor are combined.

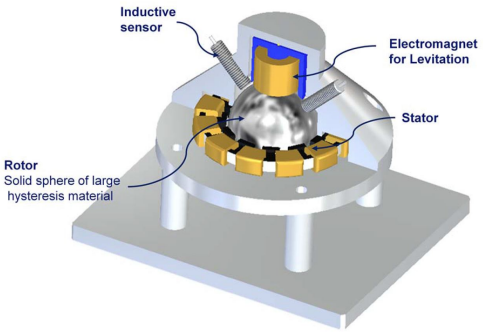

Figure 1: CAD design of 1D-MSRS.

(a) (b)

Figure 2: Photograph of the 1D-MSRS. (a) Structure; (b) stator and rotor.

We believe that the bearingless motor is a potential way to solve the field coupling between motor and bearing field for the 3D spherical motor design.

This paper focuses on the design characteristics of the suspension and driving system of the 1D-MSRS. What follows are the simulation and experimental results that demonstrate the performance of the 1D-MSRS. A more detailed analysis of the design, modeling, and control of the system is presented in [15].

II. Single DOF Reaction Sphere Design and Integration

The 1D-MSRS is a motor with a magnetically levitated spherical rotor that can rotate and stores momentum about the vertical axis.

A. System Overview

Figure 1 shows the CAD design of 1D-MSRS. The rotor is a 54 mm diameter sphere of hardened D2 steel. Four induction position sensors are placed around the rotor to measure the sphere's position in three translational degrees of freedom. The rotor sphere is magnetically levitated in the vertical direction by a reluctance actuator placed at the north pole. The stator is arranged around the sphere's equator line, and serves both for levitating the sphere in the horizontal plane and for generating torque about z axis simultaneously by a bearingless motor configuration. A reflective optical tachometer is used for speed detection of the reaction sphere. The structure of the device is presented in Figure 2.

(a) (b)

Figure 3: Stator for the 1D-MSRS without and with winding.

B. Position Sensors

The spherical rotor displacements in all three translational degrees of freedom are monitored by position sensors, which are of induction type. The four sensors are arranged 45 degrees to the vertical axis, and pointing to the center of the sphere. In this configuration the translation of the sphere in 3 directions (two horizontal directions and one vertical direction, also x, y and z) are sensed and noise is mitigated by taking the average of the signals.

C. Rotor

The rotor presents in the 1D-MSRS is a 54 mm diameter solid sphere of magnetically hard material. According to the analysis of hysteresis motor torque, the torque is proportional to rotor material's hysteresis loop area [16]. Although materials with better hysteresis properties exists, we selected D2 steel for the rotor of 1D-MSRS for the proof of our design, as this material was readily available. D2 steel is a kind of high Carbon, high Chromium type tool steel. It contains 11 to 15 percent Chromium, which makes it a deep hardening, highly wear resistant and magnetically hard alloy. These properties of the D2 steel makes it a good candidate for the rotor material of a hysteresis motor.

D. Stator

The stator for the 1D-MSRS is a custom-made stator with 24 slots and a length of 9.50 mm, which is stacking 12 layers of motor stator laminations cut from non-oriented electrical steel sheets of gauge 24. Since the stator needs to work as a magnetic bearing and motor stator simultaneously, the multiple winding approach of a bearingless motor is used, with its 4-pole winding for rotation and 2-pole winding for stabilization. Figure 3 shows the stator for the reaction sphere, where (a) shows the stator laminations without winding, and (b) shows the wound stator.

E. Vertical levitation actuator

An electromagnet actuator is used for the position control of the reaction sphere in the vertical direction. Figure 4 shows the rotor sphere being levitated in the vertical direction by this actuator.

To make the system more energy efficient, a piece of permanent magnet is embedded in the magnetic path of the levitation actuator. With this design, most of the weight is carried by the permanent magnet flux and the required excitation DC coil current can be greatly reduced.

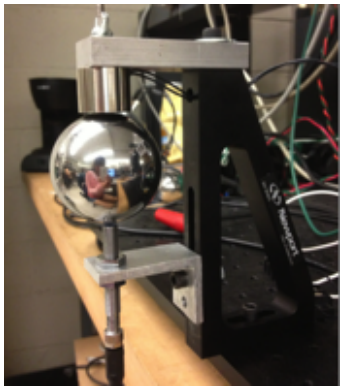

Figure 4: Single DOF levitation of sphere by reluctance actuator with permanent magnet.

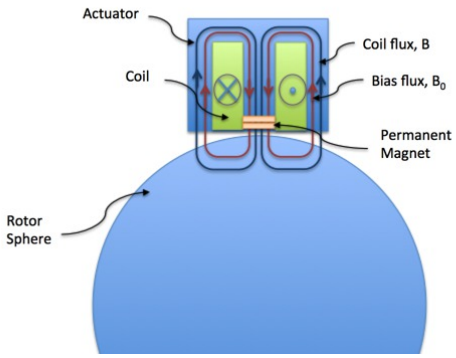

Figure 5: A cross section of the biased levitation diagram

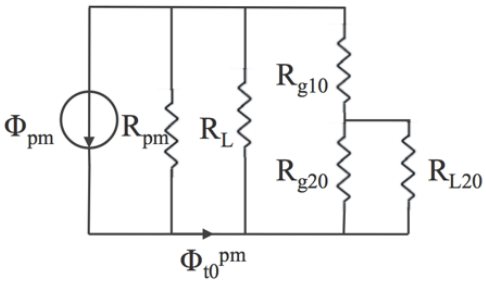

Figure 6: Equivalent magnetic circuit model for flux distribution in flux-biased levitation actuator.

F. Controller

The digital controller is selected as high speed digital signal processing computer, with the capability of hardware real-time interrupt processing. In the development of the 1D-MSRS prototype, an NI PXI chassis with real-time controller is used and is running at a sampling and processing frequency of 10 kHz. Five A/D and seven D/A converter channels with 14 bits precision are used. The controller's functions are:

- Receive signals for displacement from inductive probes and motor rotational speed from tachometer;
- Receive control commands from the host computer to change parameters of the levitation and self-bearing motor system;
- Generate and send current control signals according to the control algorithms;
- Generate acceleration trajectory for the sphere's rotation;
- Diagnose the state of the elements of the self-bearing motor system and transmit messages to the host computer.

G. Power amplifier

In order to directly drive the current in the actuators, seven separated relatively large bandwidth current control amplifiers are used. Though the driving efficiency of switching amplifier is higher, linear amplifiers are chosen in this project to avoid high frequency switching noise. The linear amplifier chip PA12 from APEX is selected, which has built-in fly-back diodes that protect the output from over voltage due to the fly-back effect. By building the current feedback loop around this amplifier for current control, a closed-loop bandwidth of 20 kHz is reached, and the amplifier can provide up to 5 A continuous current with output voltages up to ± 45 V. The design for the current control amplifiers are described in [14] in detail.

III. Single DOF Reaction Sphere Modeling and Control

In this section modeling and control of the 1D-MSRS's suspension and rotation is presented.

A. Vertical Suspension

In this section the levitation and vertical position control for the rotor sphere is introduced. Figure 5 shows a simplified diagram of the flux biased magnetic levitation actuator, which contains both bias flux from a permanent magnet and stabilizing flux generated by a coil in the slot.

First the levitation force generated by the permanent magnet is analyzed. Since the permeability of the sphere and actuator core is much larger than that of air, we assume that the magnetic reluctances are concentrated in the air gaps and in the permanent magnet. A magnetic circuit model is used to analyze the flux distribution, which is presented in Figure 6. In this model, Φ_{pm} is the remanence flux of the permanent magnet. Φ_{t0}^{pm} is the total flux that flows out from the permanent

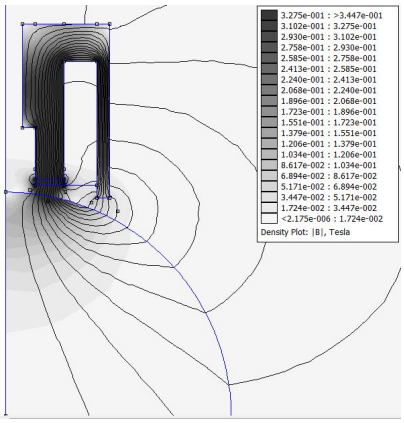

Figure 7: FEA solution of DC field in biased flux levitation actuator using typical design parameters. The permeability of the actuator core and sphere materials is assumed as $5000\mu_0$.

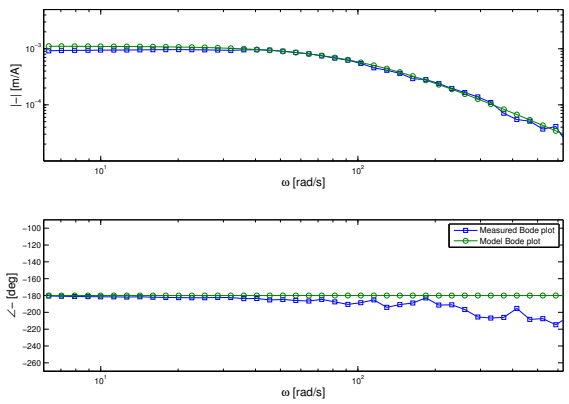

Figure 8: Plant Bode plot of the magnetic suspension system from coil current input [A] to sphere position output [m]. Blue: experimental data; green: model.

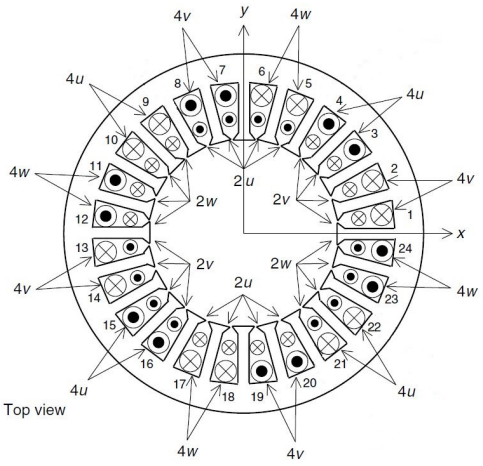

Figure 9: Multiple winding diagram for 1D-MSRS.

magnet. R_{g10} and R_{g20} are the magnetic reluctances of air gap in the center and in the periphery, respectively. R_L and R_{L20} are the reluctances for leakage paths. Here the leakage reluctance R_L is difficult to calculate using lumped parameter model, but it can be derived from numerical calculation. Figure 7 shows a flux plot calculated by the finite element method under the assumption of cylindrical symmetry. The ratio of flux leakage can be achieved from this numerical result. Then the air gap flux generated by the permanent magnet can be calculated.

In additional to the permanent magnet in the magnetic circuit, the coil in slots is excited with controlling current to levitate the sphere. The total coil winding $N \cdot i$ Ampere-turns generates controlling flux density in the air gap. By superposition of both the permanent magnet flux and the coil flux, we can calculate the total flux in the air gap, and further the reluctance force for magnetic levitation can be calculated by either an energy method or via the Maxwell stress tensor.

The frequency response from the current to the position of the rotor is measured to identify the system, and the obtained Bode plot is given in Figure 8 (Blue). An analytical modal of the magnetic suspension plant is developed, and the modeled Bode plot is shows also in Figure 8 (green). Good agreement between the model and the measured plant dynamics verified our model.

To stabilize the system, the sphere's position signal is fed back, and a PID controller is implemented in the real-time processor. A cross-over frequency of 300 $\mathrm{rad/s}$ is reached, with a phase margin of 40^o.

B. Bearingless motor

In order to drive the sphere's spinning and suspension simultaneously, a bearingless motor is adopted in the 1D-MSRS. Bearingless motor is achieved by using two sets of 3 phase winding on a single stator. By correctly configure and control current in these motor windings, the machine can generate radial force for suspension as well as torque for spinning with only one stator [17]. Figure 9 shows the winding pattern of the 1D-MSRS's stator for driving and suspension in horizontal plane.

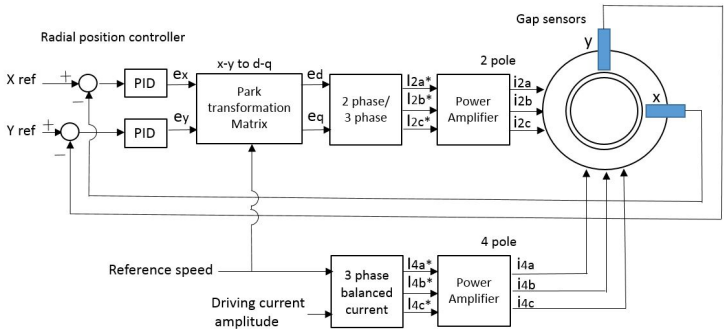

Figure 10: Bearingless motor principle diagram.

Figure 10 presents the working principle of bearingless motor. By exciting the motor winding (here the 4-pole windings) with rotational three-phase current, a torque can be created on the rotor. The air gap lengths in stationary x and y coordinates are measured by displacement sensors. Controllers are designed for lateral levitation of the sphere, and the control effort signals are transferred to rotational three-phase coordinate fixed to stator coordinate by means of Park and Clarke transformation. Then the control signals are fed into amplifiers and energizes the radial position control windings (here the 2-pole windings). Figure 10 shows the block diagram of the 1D-MSRS's bearingless motor system control.

The frequency response of the lateral position control loop is measured under different excitation current amplitude in the driving winding (here the 4 pole motor winding). The measured Bode plots is depicted in Figure 11.

Plotting the break frequencies of the plant Bode plots under different driving current amplitudes, we get the data shown in Figure 12. We fitted these data by linear function: with Eq. 1.

$$f_{break}[Hz] = 3.1429 \times I[Amp] + 3.1905. \qquad (1)$$

This changing of the break frequency of the lateral levitation plant of bearingless motor system shows that as the amplitude of the excitation strength decreases, the radial force from stator is getting smaller, thus the 'negative stiffness' in this radial

suspension system decreases. This implies that bearingless motor system requires a minimum driving current amplitude in the motor windings, even when no driving torque is needed.

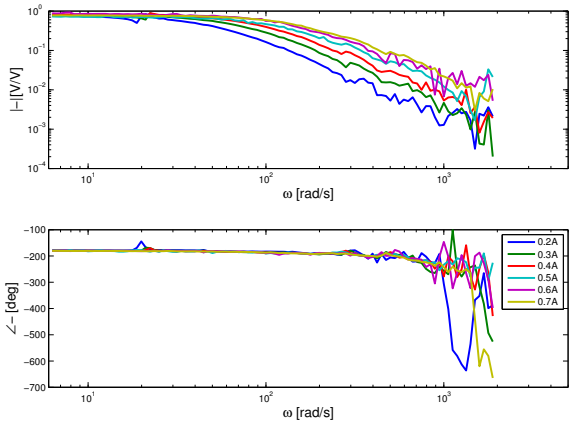

Figure 11: Experimentally measured plant frequency response for X direction sphere suspension with different excitation amplitude (zero-to-peak).

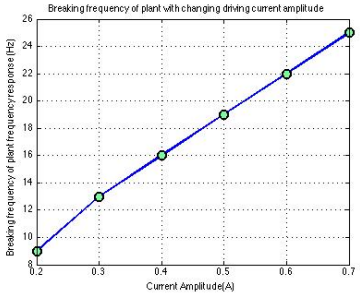

Figure 12: Break frequency of plant with changing driving current amplitude.

This change of the system's frequency response also requires an adjustment in the controller to keep the system stable under all driving conditions. To address it, PID controllers are designed to deal with this nonlinearity by adaptively adjusting its parameters according to Eq. 1. With the designed controllers, the loop reached a bandwidth varying with the excitation current amplitude and a fixed phase margin of 45 degree. The bandwidth under 0.2 A excitation current is 170 rad/s and with 0.7 A excitation the bandwidth is 471 rad/s. In this way the radial position of the sphere is successfully regulated at the center of the stator under all excitation amplitudes.

C. Hysteresis Motor

Modeling of the hysteresis motor is difficult due to the complexity of hysteresis material properties. Researchers have developed several different kinds of hysteresis motor analysis models. Reference [18] presented an analytical study of hysteresis motors and introduced the idea of using the fundamental harmonic response to the magnetizing field by simplifying the hysteresis loop into a parallelogram shape. Reference [19] introduced an elliptical hysteresis loop model and derived an equivalent circuit model for the hysteresis motor under this assumption. Several other papers [20] [21] presented different set of hysteresis motor models using the analogies to other types of motors.

In our work, an elliptical approximation of hysteresis loop is used to analyze the dynamic behavior of the 1D-MSRS, and the corresponding equivalent circuit of hysteresis motor was developed by Miyairi and T. Kataoka [19] and further presented in [22] and [14]. This model is used to analyze both the steady state running and starting up of the reaction sphere, and we believe it is reasonable for several reasons. First, we are using the self-bearing motor for the lateral suspension of the 1-D MSRS, thus the sphere is always first levitated in radial directions and then being driven by rotating magnetic field. In this way, under DC excitation conditions or rotating under the excitation of rotating magnetic field, the magnetization pattern and pole distribution of the sphere surface is the same. Therefore we do not need to model the virgin magnetization curve (B-H curve starting from zero magnetization) as most hysteresis motor transient simulation does. Second, the reaction sphere is excited below saturation. In this circumstance the real hysteresis loop has less higher order harmonics, which makes it more similar to a phase lag between B field and H field. Third, due to the effect of eddy current, the hysteresis property is showing dependency to excitation frequency. The loop widening effect makes the hysteresis loop get more close to an elliptical model. Last, this model has an assumption that the hysteresis lag angle is held constant and is equal to it's maximum when slip is large, which makes the motor hysteresis starting torque maximum and does not depend on slip during starting up. This assumption is close to what is really happening when a hysteresis motor is starting spinning, and makes this equivalent circuit model valid for motor transient behavior simulation, although usually they are not accurate when slip is large.

In the hysteresis motor's equivalent circuit model, a balanced single-frequency, three-phase source is assumed. The B-H curve of the rotor material is approximated by a ellipse:

$$B = B_m cos(\theta) \tag{2a}$$

$$H = \frac{B_m}{\mu} cos(\theta + \delta). \tag{2b}$$

Here δ is the lag angle between H and B. Thus the permeability μ is the ratio of the maximum value of B and H is $\mu = \frac{B_m}{H_m}$. Higher order harmonics of the flux density are neglected. Based on these assumptions, the motor equations can be derived, and Figure 13 shows the motor equivalent circuit. The values of the circuit elements derived in [19] are:

$$L_g = \frac{2mK_w{}^2N^2\mu_0 lRg}{p^2\pi g} \tag{3a}$$

$$R_r = \omega_b \frac{mK_w{}^2N^2V_r\mu}{\pi^2 r_r{}^2} sin\delta \tag{3b}$$

$$L_r = \omega_b \frac{mK_w{}^2N^2V_r\mu}{\pi^2 r_r{}^2} cos\delta \tag{3c}$$

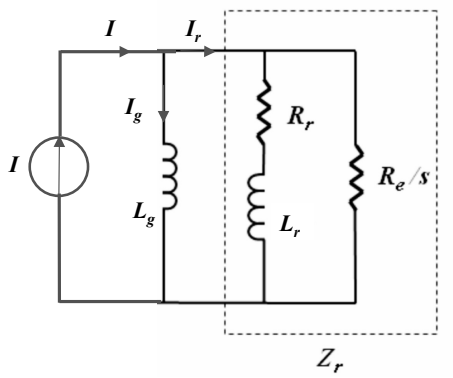

Figure 13: Equivalent circuit model of hysteresis motor.

Here δ is the lag angle; K_w is the winding factor; m is the number of phase;p is the number of poles; r_r is mean radius of length of the magnetic field path within rotor; r_g is the radius of the air gap; ω_b is the input angular frequency; N is the number of winding per phase; g is the air gap length; and μ is the permeability of the rotor material.

After solving the circuit for apparent currents, we can calculate the electrical torque of the motor by:

$$T_e = \frac{m}{2}\frac{P}{2}L_g I_r I_g sin\delta \tag{4}$$

Then the motor's mechanical speed is calculated by the rotor's dynamic equation:

$$T_e - T_d = \frac{J}{p}\frac{dw_r}{dt} \tag{5}$$

The lag angle between electrical angular position and mechanical angular position is given by:

$$\frac{\omega_b - \omega_r}{p} = \frac{d\delta}{dt} \tag{6}$$

Simulation of the reaction sphere's dynamics can be conducted by selecting initial conditions and the above calculations. Matlab/Simulink is used for the simulation of the motor system, and the results are reported in the later section.

IV. Experimental and Simulation Results

Table I shows the design parameters for the 1D-MSRS.

Table I: Parameters for equivalent circuit model simulation

parameter	value
Sphere radius	27 mm
Stator height	9.5 mm
Stator back iron length	12mm
Stator pole width	3 mm
Air gap length between stator and sphere (each side)	0.4 mm
Stator number of slots	24
Number of poles for driving winding	4
Number of wires per slot for driving winding	80
Number of poles for suspension winding	2
Number of wires per slot for suspension winding	40

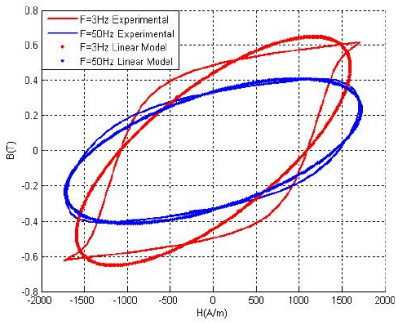

Figure 14: D2 steel linear model approximation from [14].

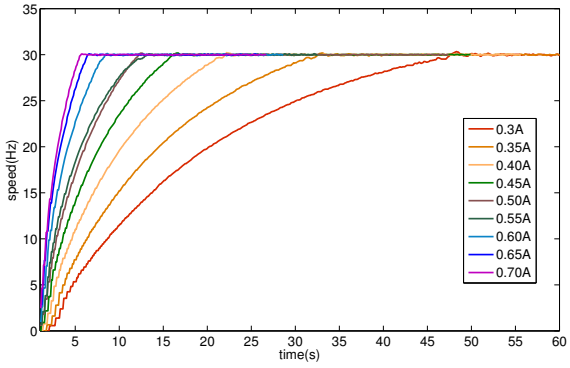

Figure 15: Acceleration curves of 1D-MSRS under different excitation current amplitude.

The B-H characteristics of the sphere material are required for the simulation of the reaction sphere. As we discussed before, the hysteresis loop has a dependency on the excitation frequency. Figure 14 presents the B-H curve of the rotor material (D2 steel) under different excitation frequencies, and their linearized elliptical models. The original data and the measuring process are given in [14]. We chose the appropriate permeability μ and lag angle δ for simulation according to the measurement under certain frequency with taking the loop widening effect into account.

Figure 15 presents the acceleration curves of the 1D-MSRS under different amplitudes of excitation current. We can see

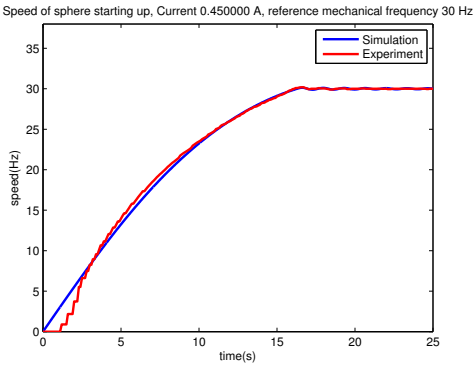

Figure 16: Starting angular speed data under excitation current of peak value 0.45 A.

that all curves locks into the reference speed of 30 Hz (1800 rpm) after acceleration, and a $3-5$ Hz speed oscillation occurs when the speed reaches synchronous. THis is due to the hunting dynamics of the hysteresis motor. Data shows that with 0.7 A excitation current, the sphere can reach the synchronous speed of 30 Hz (1800 rpm) within 6 seconds. Also, a starting torque of $8.15 \times 10^{-3} N.m$ is demonstrated under 0.7 A exciting current.

The maximum achievable speed for the 1D-MSRS is also tested.When running in the lab with the existence of air drag, the sphere can run up to 200 Hz (12,000 rpm) synchronous speed. We believe this specification can be improved when the sphere is running in vacuum.

Figure 16 shows the measured and simulated starting angular speed of the 1D-MSRS plotting together. Good agreement between simulation and experimental data confirms the validity of the equivalent circuit model for analysis of the 1D-MSRS.

V. Conclusion and Future Work

The development of a magnetically suspended reaction sphere based on a single degree-of-freedom hysteresis drive (1D-MSRS) is presented in this paper. Magnetic suspension, bearingless drive and hysteresis motor principles are used in the design for 1D-MSRS. An equivalent circuit model for hysteresis motor is used to analyze the dynamic behavior of the 1D-MSRS. A starting torque of 8.15 mNm is achieved under 0.7 A of excitation current. The sphere can run up to 200 Hz (12,000 rpm) synchronous speed in lab.

Further research on speed hunting suppression, power efficiency optimization and motor performance tests in closed-loop speed control for the 1D-MSRS is ongoing in the Precision Motion Control Lab at MIT.

With these results in hand, the next steps to take in the future would be the design of a three dimensional reaction sphere. This study shows that hysteresis motor is a promising motor concept for space application, especially when it is assisted with magnetic bearings. It enables vibration-free operations and a very high rotational speed. The performance of the 1D-MSRS demonstrates that bearingless motor is a promising method to solve the field coupling between motor and bearing function for a 3D magnetic levitated motor. Through the tests of the 1D-MSRS also shows that with its advantages of high-speed, quiet operation and self-starting, hysteresis motor is a promising motor concept for reaction wheel applications.

Acknowledgment

The authors would like to thank MIT Lincoln Laboratory for supporting this project via the Advanced Concept Committee. We also thank National Instruments for equipment donations for the project.

References

[1] I. A. Budianto and J. R. Olds, "Design and deployment of a satellite constellation using collaborative optimization," *Journal of spacecraft and rockets*, vol. 41, no. 6, pp. 956–963, 2004.

[2] B. Bialke, "High fidelity mathematical modeling of reaction wheel performance," *Guidance and control 1998*, pp. 483–496, 1998.

[3] T. Marshall, T. Gunderman, and F. Mobley, "Reaction wheel control of the msx satellite," in *Guidance and Control 1991*, vol. 1, 1991, pp. 119–138.

[4] L. P. Davis, J. Wilson, R. Jewell, and J. Roden, "Hubble space telescope reaction wheel assembly vibration isolation system," *NASA Marshall Space Flight Center, Huntsville, Alabama*, vol. 9, 1986.

[5] T. Fukada, H. Hosokai, and N. Yajima, "Flexibility control of solar battery arrays: 3rd report vibration and attitude control with consideration of the dynamics of a reaction wheel as an actuator," *Bulletin of JSME*, vol. 29, no. 255, pp. 3121–3125, 1986.

[6] W. H. Isely, "Magnetically supported and torqued momentum reaction sphere," Sep. 16 1986, uS Patent 4,611,863.

[7] K. Kaneko, I. Yamada, and K. Itao, "A spherical dc servo motor with three degrees of freedom," *Journal of dynamic systems, measurement, and control*, vol. 111, pp. 398–402, 1989.

[8] G. J. Vachtsevanos and K. R. Davey, "Spherical motor particularly adapted for robotics," Apr. 19 1988, uS Patent 4,739,241.

[9] C. Xia, H. Li, and T. Shi, "3-d magnetic field and torque analysis of a novel halbach array permanent-magnet spherical motor," *Magnetics, IEEE Transactions on*, vol. 44, no. 8, pp. 2016–2020, 2008.

[10] K.-M. Lee, G. Vachtsevanos, and C. Kwan, "Development of a spherical stepper wrist motor," *Journal of Intelligent and Robotic Systems*, vol. 1, no. 3, pp. 225–242, 1988.

[11] K.-M. Lee, H. Son, J. Joni *et al.*, "Concept development and design of a spherical wheel motor (swm)," in *IEEE International Conference on Robotics and Automation*, vol. 4. IEEE; 1999, 2005, p. 3652.

[12] W. Wang, J. Wang, G. Jewell, and D. Howe, "Design and control of a novel spherical permanent magnet actuator with three degrees of freedom," *Mechatronics, IEEE/ASME Transactions on*, vol. 8, no. 4, pp. 457–468, 2003.

[13] E. Onillon, O. Chételat, L. Rossini, L. Lisowski, S. Droz, and J. Moerschell, "Reaction sphere for attitude control," in *Proc. 13th European Space Mechanisms and Tribology Symposium*, 2009.

[14] M. Imani Nejad, "Self-bearing motor design & control," Ph.D. dissertation, Massachusetts Institute of Technology, 2013.

[15] L. Zhou, "Magnatically suspended reaction sphere with one-axis hysteresis drive," Master's thesis, Massachusetts Institute of Technology, 2014.

[16] B. R. Teare, "Theory of hysteresis-motor torque," *Electrical Engineering*, vol. 59, no. 12, pp. 907–912, 1940.

[17] A. Chiba, T. Fukao, O. Ichikawa, M. Oshima, M. Takemoto, and D. G. Dorrell, *Magnetic bearings and bearingless drives*. Access Online via Elsevier, 2005.

[18] M. Copeland and G. Slemon, "An analysis of the hysteresis motor i-analysis of the idealized machine," *Power Apparatus and Systems, IEEE Transactions on*, vol. 82, no. 65, pp. 34–42, 1963.

[19] S. Miyairi and T. Kataoka, "A basic equivalent circuit of the hysteresis motor," *Elect. Engng. Japan (USA)*, vol. 85, pp. 41–50, 1965.

[20] M. A. Rahman, "Analytical models for polyphase hysteresis motor," *Power Apparatus and Systems, IEEE Transactions on*, no. 1, pp. 237–242, 1973.

[21] D. O'Kelly, "Theory and performance of solid-rotor induction and hysteresis machines," in *Proceedings of the Institution of Electrical Engineers*, vol. 123, no. 5. IET, 1976, pp. 421–428.

[22] J. Nitao, E. Scharlemann, and B. Kirkendall, "Equivalent circuit modeling of hysteresis motors," Lawrence Livermore National Laboratory (LLNL), Livermore, CA, Tech. Rep., 2009.